J. Materials, Conc. Struct. Pavements, JSCE, No. 725/V-58, 293-304, 2003 February

DEVELOPMENT OF CONCRETE CONSTITUTIVE LAWS BASED ON 3D LATTICE EQUIVALENT CONTINUUM

Syed Ishtiaq AHMAD[1] and Tada-aki TANABE[2]

[1] Member of JSCE, Grad. Student, Dept. of Civil Eng., Nagoya University
(Furo-cho, Chikusa-ku, Nagoya, 464-8603,Japan)
[2] Member of JSCE, Dr. Eng., Professor, Dept. of Civil Eng., Nagoya University
(Furo-cho, Chikusa-ku, Nagoya, 464-8603,Japan)

Robust and engineering oriented three-dimensional concrete constitutive laws are formulated from equivalent continuum of lattice system. Two approaches are taken to develop these constitutive laws: one from known strain field i.e. kinematic constraint and other from known stress field i.e. static constraint; later one to incorporate poisson's ratio in the rigidity matrix. Methods are also proposed to establish the stress-strain behavior of individual concrete lattices. Finally, the developed constitutive laws are applied to analyze biaxial and triaxial test results of various researchers. Analysis results show close approximation of test data, which indicates the effectiveness of these proposed constitutive laws.

Key Words: *concrete, lattices, constitutive equations, Triaxial stresses,Three-dimensional Models, Poisson's ratio*

1. INTRODUCTION

Three-dimensional (3D) analysis of concrete structures is increasingly replacing two-dimensional (2D) analysis with the rapid advancement and easy availability of high speed computing hardware. Simultaneously, the formulation of 3D-generalized constitutive equations is becoming an important aspect of research, as use of appropriate constitutive laws form the basis for analytical results to conform to the experimental results closely. A review of the literature shows that only a few models for full 3D analysis of reinforced concrete has been reported. A comparative listing given in Selby and Vecchio[1)] indicates that the few published studies differ in their choice of triaxial constitutive laws of concrete, treatments of cracking behavior, modeling of steel reinforcement as well as numerical procedures in solving the governing equations. Therefore, the authors of this paper feel that there is room for comprehensive improvement in this area. The authors also believe that any research in this area should be to benefit the profession so that the existing gap between scientific activity and practice become narrowed. It is therefore of interest to develop constitutive laws for reinforced concrete that will not only give reasonably accurate results but will also provide clear and easy understanding of the complex phenomenon occurring inside concrete elements with respect to stress and strain distribution i.e. more engineering oriented constitutive laws as opposed to prevailing constitutive laws of concrete. For this, the concept of equivalent continuum of lattice system[2)] is used and extended for three dimensions.

The lattice equivalent continuum model, hereafter *LECM*, grows from the successful use of discreet lattice modeling of reinforced concrete element by Niwa et al.[3)]. The continuum model essentially retains the features of uniaxiality of stress bearing materials, however, combination of those alters their fundamental characteristics from initially orthotropic model and later even to general anisotropic model retaining symmetry of the constitutive equation. This gives freedom of expressing the complex characteristics of the reinforced concrete elements with simple uniaxial lattice elements. Concepts behind the formulation of *LECM* are unique and different from other well known uniaxial type models like Bazant's Microplane model[4)]. For instance, number of microplanes used in Bazant's model is far more than the lattices used for modeling reinforced concrete in *LECM*. Therefore, the present model is far simpler for understanding and application. Furthermore, appropriate peak stress and strain criterion for individual lattices makes *LECM* model distinct from Microplane model where stress strain laws are not the ones for macroscopic concrete elements.

In the present paper, generalized three dimensional constitutive laws are developed based on *LECM*. For this, two approaches are considered: one with kinematic constraints i.e. from the known strain field and the other with static constraints, i.e. from known stress field. The two approaches have fundamental differences in a sense that strain in the lattices formed in the model based on kinematic constraint are independent of the surrounding lattices. While, in case of static constraint, the strains in lattices are related with that of the surrounding lattices by poisson's ratio. This difference will become more apparent in the subsequent sections of this paper.

To evaluate the failure stress of concrete lattices in 3D stress space, the failure surface proposed by Kang and Willam[5), 6)] has been used. Tangent value of the nonlinear elastic modulus of concrete lattices is evaluated from the stress-strain curve proposed by Sargin[7)] and poisson's ratio, for the case of static constraints, are changed appropriately. The most attractive feature of these developed constitutive laws is the simplicity and easiness in its use. These models also provide good and clear understanding of the complex characteristics of the stress strain behavior inside concrete elements. Comparison with biaxial and triaxial test results of several authors that will be presented in this paper indicates that developed constitutive laws are applicable to all kinds of stress states.

2. FORMULATION OF THE CONSTITUTIVE EQUATION

In the formulation for constitutive laws of concrete in *LECM*, reinforced concrete is assumed as cracked and composed of steel and concrete lattices. The stresses and direction of the steel lattices are those of reinforcing steel itself, while crack directions in concrete, which is fixed by principal stresses, determine concrete lattices and their orientation. **Fig.1** shows schematic lattice idealization in cracked concrete. Although the present formulation is based on cracked reinforced concrete, it can easily be extended to uncracked reinforced and plain concrete as well. Two derivations are subsequently presented in this section, one from known strain field i.e. kinematic constraints and the other from known stress field i.e. static constraints.

Since constitutive matrix formed from static constraint approach contains one additional parameter, i.e. poisson's ratio, it is apparent that this approach will result in more complete and comprehensive constitutive laws than kinematic constraint approach. However, kinematic approach is the traditional form of *LECM* that has been used successfully over the years to analyze structures in 2D for both static and

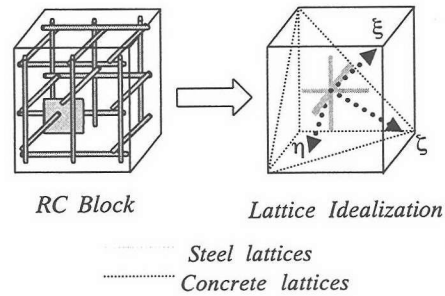

(a) Lattices in Reinforced Concrete

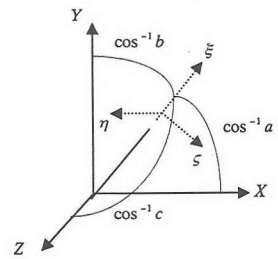

(b) Local Coordinate in a Lattice Unit

Fig.1 Lattice in Uniform Strain Field

cyclic loading[2)]. Hence, both of these approaches are investigated in this paper.

(1) Kinematic Constraints

We begin assuming uniformly strained 3D continuum strain of which read in the global coordinate,

$$\{\varepsilon_g\}=[\varepsilon_x \quad \varepsilon_y \quad \varepsilon_z \quad \gamma_{sy} \quad \gamma_{yz} \quad \gamma_{zx}]^T \qquad (1)$$

The strain in a lattice member in this strain field is assumed to be identical with the strain of Eq.(1). Therefore, for an inclined member of lattice for which local coordinate (ξ, η, ζ) is taken such that ξ coordinate coincide with lattice axis, lattice strain ε_ξ reads,

$$\varepsilon_\xi = [a^2 \quad b^2 \quad c^2 \quad a\,b \quad b\,c \quad c\,a] \begin{Bmatrix} \varepsilon_x \\ \varepsilon_y \\ \varepsilon_z \\ \gamma_{xy} \\ \gamma_{yz} \\ \gamma_{zx} \end{Bmatrix} \qquad (2)$$

Where a, b and c are directions cosines of the lattice direction with respect to x, y and z axis as shown in **Fig.1(b)**. For reinforced concrete, ξ, η and ζ are the

directions of principal strains and can be computed using basic continuum mechanics laws. If n number of lattices exists in the continuum we can write,

$$\{\varepsilon_l\} = [L_\varepsilon]\{\varepsilon_g\} \tag{3}$$

where,

$$[L_\varepsilon] = \begin{bmatrix} a_1^2 & b_1^2 & c_1^2 & a_1b_1 & b_1c_1 & c_1a_1 \\ \cdots & \cdots & \cdots & \cdots & \cdots & \cdots \\ a_j^2 & b_j^2 & c_j^2 & a_jb_j & b_jc_j & c_ja_j \\ \cdots & \cdots & \cdots & \cdots & \cdots & \cdots \\ a_n^2 & b_n^2 & c_n^2 & a_nb_n & b_nc_n & c_na_n \end{bmatrix} \tag{4}$$

Multiplying strains with stiffness of each lattice, the incremental stresses of the replaced continuum can be evaluated as,

$$\{\Delta\sigma_l\} = \begin{Bmatrix} \Delta\sigma_{l1} \\ \vdots \\ \Delta\sigma_{lj} \\ \vdots \\ \Delta\sigma_{ln} \end{Bmatrix} = \begin{bmatrix} r_1 & & & & \\ & \ddots & & 0 & \\ & & r_j & & \\ & 0 & & \ddots & \\ & & & & r_{nn} \end{bmatrix} \begin{Bmatrix} \Delta\varepsilon_{l1} \\ \vdots \\ \Delta\varepsilon_{lj} \\ \vdots \\ \Delta\varepsilon_{ln} \end{Bmatrix}$$

$$= [R_n]\{\Delta\varepsilon_l\} \tag{5}$$

Where, $r_j = \partial\sigma_j / \partial\varepsilon_j$, denotes the tangential stiffness of individual lattices.

Continuum local stresses transformed to global coordinate has the following form:

$$\begin{Bmatrix} \Delta\sigma_x \\ \Delta\sigma_y \\ \Delta\sigma_z \\ \Delta\tau_{xy} \\ \Delta\tau_{yz} \\ \Delta\tau_{zx} \end{Bmatrix} = \begin{bmatrix} a_j^2 \\ b_j^2 \\ c_j^2 \\ a_jb_j \\ b_jc_j \\ c_ja_j \end{bmatrix} \{\Delta\sigma_l\} \tag{6}$$

Summing over all lattices, gives the expression,

$$\{\Delta\sigma_g\} = \begin{Bmatrix} \Delta\sigma_x \\ \Delta\sigma_y \\ \Delta\sigma_z \\ \Delta\tau_{xy} \\ \Delta\tau_{yz} \\ \Delta\tau_{zx} \end{Bmatrix} = \begin{bmatrix} a_1^2 & \cdots & a_j^2 & \cdots & a_n^2 \\ b_1^2 & \cdots & b_j^2 & \cdots & b_n^2 \\ c_1^2 & \cdots & c_j^2 & \cdots & c_n^2 \\ a_1b_1 & \cdots & a_jb_j & \cdots & a_nb_n \\ b_1c_1 & \cdots & b_jc_j & \cdots & b_nc_n \\ c_1a_1 & \cdots & c_ja_j & \cdots & c_na_n \end{bmatrix} \{\Delta\sigma_l\} \tag{7}$$

which can be written as,

$$\begin{aligned} \{\Delta\sigma_g\} &= [L_\varepsilon]^T\{\Delta\sigma_l\} \\ &= [L_\varepsilon]^T[R_n][L_\varepsilon]\{\Delta\varepsilon_g\} \\ &= [D_{kin}]\{\Delta\varepsilon_g\} \end{aligned} \tag{8}$$

where,

$$[D_{kin}] = \begin{bmatrix} \sum_1^n r_j a_j^4 & \sum_1^n r_j a_j^2 b_j^2 & \sum_1^n r_j a_j^2 b_j^2 & \sum_1^n r_j a_j^3 b_j & \sum_1^n r_j a_j^2 b_j c_j & \sum_1^n r_j a_j^3 c_j \\ & \sum_1^n r_j a_j^4 & \sum_1^n r_j b_j^2 c_j^2 & \sum_1^n r_j b_j^3 a_j & \sum_1^n r_j b_j^3 c_j & \sum_1^n r_j a_j b_j^2 c_j \\ & & \sum_1^n r_j c_j^4 & \sum_1^n r_j a_j b_j c_j^2 & \sum_1^n r_j c_j^3 b_j & \sum_1^n r_j c_j^3 a_j \\ & & & \sum_1^n r_j a_j^2 c_j^2 & \sum_1^n r_j a_j b_j^2 c_j & \sum_1^n r_j a_j^2 b_j^2 c_j \\ & Sym & & & \sum_1^n r_j b_j^2 c_j^2 & \sum_1^n r_j c_j^2 b_j a_j \\ & & & & & \sum_1^n r_j c_j^2 a_j^2 \end{bmatrix} \tag{9}$$

Eq. (9) is the general form of the constitutive matrix for lattice equivalent continuum based on kinematic constraint. Note that for reinforced concrete, number of lattices in any calculation point would be six. Of those, three will represent principal strain direction of concrete while other three will model reinforcement of three global directions in 3D strain space.

(2) Static Constraint

In static constraint method, lattice equivalent continuum constitutive matrix is formulated from known stress field. In this way, the developed constitutive matrix contains poisson's ratio, which is the basic difference from the rigidity matrix derived from kinematic constraint method. The procedure for derivation can be summarized as: first we identify concrete and steel lattices in the known stress field. We then proceed by treating them separately and finally, we combine them using the condition of strain compatibility.

When there is an increase of $\{\Delta\sigma_g\}$ in global stress field, there is corresponding increase in concrete and reinforcement stresses according to their effective stress bearing area. Suppose, increase in concrete stress is $\Delta\sigma_c$, and that of reinforcement is $\Delta\sigma_s$. Therefore, we get,

$$\{\Delta\sigma_g\} = \{\Delta\sigma_c\} + \{\Delta\sigma_s\} \tag{10}$$

Next we evaluate the increase in principal stresses of concrete and steel due to increase in $\Delta\sigma_c$ and $\Delta\sigma_s$, respectively. For concrete, this is evaluated by taking

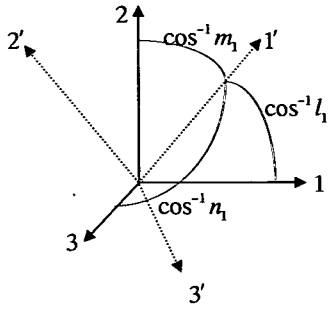

1,2 *and* 3 *are steel lattice directions*

1',2' *and* 3' *are concrete lattice directions*

Fig.2 Steel and Concrete Lattices with their Orientations

difference between principal stresses of total stress field before and after stress increment. Principal stresses of any stress field can be found by evaluating the roots of the following equation:

$$\sigma_c^3 - I_1\sigma_c^2 + I_2\sigma_c - I_3 = 0 \qquad (11)$$

Where, I_1, I_2 and I_3 are three stress invariants (given by the following relations: $I_1 = \sigma_c^{(1)} + \sigma_c^{(2)} + \sigma_c^{(3)}$; $I_2 = \sigma_c^{(1)}\sigma_c^{(2)} + \sigma_c^{(2)}\sigma_c^{(3)} + \sigma_c^{(3)}\sigma_c^{(1)}$; $I_3 = \sigma_c^{(1)}\sigma_c^{(2)}\sigma_c^{(3)}$ where, $\sigma_c^{(1)}, \sigma_c^{(2)}$ and $\sigma_c^{(3)}$ are three concrete principal stresses) and σ_c denotes total concrete stress field. Let us assume the incremental principal stress vector of concrete as $\Delta\sigma_c^{(p)} = \{\Delta\sigma_c^{(1)}, \Delta\sigma_c^{(2)}, \Delta\sigma_c^{(3)}\}^T$. Note that these principal stresses denote the increase in concrete lattice stresses of the system itself. Orientation of these lattices with respect to global axis system can be evaluated using the following relation:

$$\left(\sigma_{ij} - \sigma^{(k)}\delta_{ij}\right) n_j^{(k)} = 0 \qquad (12)$$

where, $n_j^{(k)}$ is the vector denoting direction cosines for the lattice with stress $\sigma^{(k)}$. Here superscript *(k)* denotes principal stress directions *1,2* or *3*; *i* and *j* have ranges from 1 to 3. And σ_{ij} is the stress vector. The letter subscripts and superscripts used enclosed by parentheses are merely labels and as such do not participate in any summation process. Magnitude and orientation of steel lattices incremental stresses, $\Delta\sigma_s^{(p)} = \left\{\Delta\sigma_s^{(1)} \quad \Delta\sigma_s^{(2)} \quad \Delta\sigma_s^{(3)}\right\}^T$ are those of reinforcing steel it self.

Now, we get, corresponding concrete lattice strains incorporating poisson's ratio:

$$\left\{\Delta\varepsilon_c^{(p)}\right\} = \begin{Bmatrix}\Delta\varepsilon_c^{(1)}\\ \Delta\varepsilon_c^{(2)}\\ \Delta\varepsilon_c^{(2)}\end{Bmatrix} = \begin{bmatrix} \frac{1}{E_{ct}^{(1)}} & -\frac{\nu^{(2)}}{E_{ct}^{(2)}} & -\frac{\nu^{(3)}}{E_{ct}^{(3)}} \\ -\frac{\nu^{(1)}}{E_{ct}^{(1)}} & \frac{1}{E_{ct}^{(2)}} & -\frac{\nu^{(3)}}{E_{ct}^{(3)}} \\ -\frac{\nu^{(1)}}{E_{ct}^{(1)}} & -\frac{\nu^{(2)}}{E_{ct}^{(2)}} & \frac{1}{E_{ct}^{(3)}} \end{bmatrix} \begin{Bmatrix}\Delta\sigma_C^{(1)}\\ \Delta\sigma_C^{(2)}\\ \Delta\sigma_C^{(3)}\end{Bmatrix}$$
$$= [C_c]\left\{\Delta\sigma_c^{(p)}\right\} \qquad (13)$$

and, corresponding steel lattice incremental strain,

$$\left\{\Delta\varepsilon_s^{(p)}\right\} = \begin{Bmatrix}\Delta\varepsilon_s^{(1)}\\ \Delta\varepsilon_s^{(2)}\\ \Delta\varepsilon_s^{(3)}\end{Bmatrix} = \begin{bmatrix} \frac{1}{E_{st}^{(1)}} & 0 & 0 \\ 0 & \frac{1}{E_{st}^{(2)}} & 0 \\ 0 & 0 & \frac{1}{E_{st}^{(3)}} \end{bmatrix} \begin{Bmatrix}\Delta\sigma_s^{(1)}\\ \Delta\sigma_s^{(2)}\\ \Delta\sigma_s^{(3)}\end{Bmatrix}$$
$$= [C_s]\left\{\Delta\sigma_s^{(p)}\right\} \qquad (14)$$

E_{ct} and E_{st} are concrete and steel tangent modulus. Strain compatibility requires that,

$$\left\{\Delta\varepsilon_s^{(p)}\right\} = [T_s]\left\{\Delta\varepsilon_c^{(p)}\right\} \qquad (15)$$

which implies perfect bonding between steel and concrete lattices. An offset of this limitation may be done making adjustment to concrete and steel tangent modulus. However, that is ignored in this work. Here, $[T_s]$ is the matrix to transform strain from concrete lattice to the direction of steel lattice and have the form,

$$[T_s] = \begin{bmatrix} l_1^2 & m_1^2 & n_1^2 \\ l_2^2 & m_2^2 & n_2^2 \\ l_3^2 & m_3^2 & n_3^2 \end{bmatrix} \qquad (16)$$

and, l, m and n are direction cosines as shown in **Fig.2**.

Now, the total stress is given by Eq.(10) can be written

$$\begin{aligned}\left\{\Delta\sigma_g\right\} &= \left\{\Delta\sigma_c\right\} + \left\{\Delta\sigma_s\right\} \\ &= [T_{pc}]\left\{\Delta\sigma_c^{(p)}\right\} + [T_{ps}]\left\{\Delta\sigma_s^{(p)}\right\} \\ &= [T_{pc}][C_c]^{-1}\left\{\Delta\varepsilon_c^{(p)}\right\} + [T_{ps}][C_s]^{-1}\left\{\Delta\varepsilon_s^{(p)}\right\} \\ &= [T_{pc}][C_c]^{-1}\left\{\Delta\varepsilon_c^{(p)}\right\} + [T_{ps}][C_s]^{-1}[T_s]\left\{\Delta\varepsilon_c^{(p)}\right\} \\ &= \left\{[T_{pc}][C_c]^{-1} + [T_{ps}][C_s]^{-1}[T_s]\right\}\left\{\Delta\varepsilon_c^{(p)}\right\} \\ &= \left\{[T_{pc}][C_c]^{-1} + [T_{ps}][C_s]^{-1}[T_s]\right\}[T_c]\left\{\varepsilon_g\right\} \\ &= [D_{stat}]\left\{\Delta\varepsilon_g\right\}\end{aligned} \qquad (17)$$

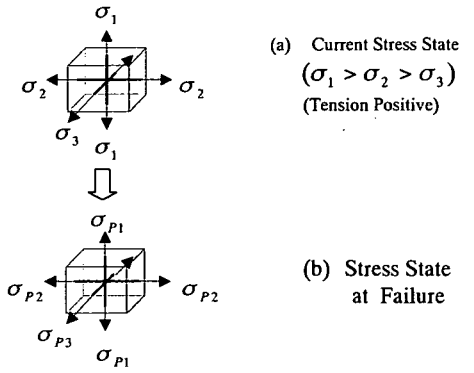

Fig.3 Concrete Lattices traced out by Principal stresses in an element that contribute to the continuum

Also, $[T_{pc}]$ and $[T_{ps}]$ are transformation matrix from principal concrete and steel direction, respectively, to global (x,y,z) direction and has the following form,

$$\begin{bmatrix} l_1^2 & l_2^2 & l_3^2 \\ m_1^2 & m_2^2 & m_3^2 \\ n_1^2 & n_2^2 & n_3^2 \\ l_1m_1 & l_2m_2 & l_3m_3 \\ m_1n_1 & m_2n_2 & m_3n_3 \\ n_1l_1 & n_2l_2 & n_3l_3 \end{bmatrix}$$

Where l, m and n's are direction cosines between principal stress direction and global (x,y,z) direction respectively. $[T_C]$ being the transformation matrix from concrete strain direction to global direction. Therefore, the constitutive matrix considering main lattices can be given as,

$$[D_{stat}] = \{[T_{pc}][C_c]^{-1} + [T_{ps}][C_s]^{-1}[T_s]\}[T_c] \quad (18)$$

As can be seen, evaluation of constitutive matrix for reinforced concrete system using simple *LECM* equations (9) or (18) only requires knowledge of orientation and stiffness of individual steel and concrete lattices.

3. PEAK STRESS CRITERION

Stress strain relation of any concrete principal stress i.e. lattice direction will be influenced by the stresses in other two principal stresses, i.e. lattice directions. Additionally, peak strength of concrete uniaxial stress-strain curves will also vary due to stresses in other two principal directions. In the analysis, prior

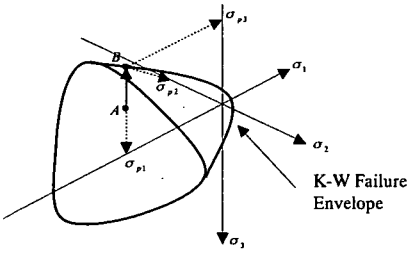

Fig. 4 Failure Stress Criteria with Kang-Willam[5),6)] Failure Surface

estimation of these peak stresses considering stress influence from other two directions is necessary because peak stress point fixes the overall shape of the stress-strain curve and therefore, affect the tangent modulus value to be incorporated in Eqn.(9) and (18). For estimating the influence of stresses from other two directions, stress paths at any point up to failure state is needed to be known. However, it should be noted that there are infinite number of stress paths in which the failure stress state can be achieved by changing the current stresses in individual lattices. But for this present study, it is assumed that failure is achieved by decreasing stress in the minimally stressed lattice (i.e. σ_3 for the element shown in **Fig.3**) while keeping other two direction fixed. This type of failure point estimation has also been considered previously by some researchers (e.g. Ottosen[8)]). The procedure is illustrated in **Fig.4**, where point A represent the current stress state of **Fig.3(a)**. Point B, which lies in the failure surface, represent failure stress state of **Fig.3(b)** and is achieved by decreasing σ_3, shown by the straight line from A to B. The stress state at B $(\sigma_{p1}, \sigma_{p2}, \sigma_{p3})$ is the analytical peak point for individual stress strain relation for each of the lattices.

This adopted procedure is merely an assumption among numerous ways failure can be achieved. However, one reason behind choosing this option is because it's close representation of triaxial cylinder tests that are analyzed in this paper as examples. In these tests, failure is achieved by increasing compressive load in one direction, while loads are kept constant in other two lateral directions.

The C^1-continuous failure surface proposed by Kang and Willam[5),6)] has been used as the criteria for concrete failure in this study. The curvilinear failure envelope, according to their proposed formulation, is a function of the stress invariants I_1 along with second and third deviatoric stress invariants J_2 and J_3 $\left(J_2 = \frac{1}{6}\left[\{\sigma_c^{(1)} - \sigma_c^{(2)}\}^2 + \{\sigma_c^{(2)} - \sigma_c^{(3)}\}^2 + \{\sigma_c^{(3)} - \sigma_c^{(1)}\}^2\right]\right.$, $J_3 = \sigma_c^{(1)}\sigma_c^{(2)}\sigma_c^{(3)}$ where, $\sigma_c^{(1)}, \sigma_c^{(2)}$ and $\sigma_c^{(3)}$ are concrete principal stresses) that are expressed in terms

of the Haigh-Westergaard coordinates, $\xi = I_1/\sqrt{3}$, $\rho = \sqrt{2J_2}$, and $\theta = (1/3)\cos^{-1}\{(3\sqrt{3}J_3/(2J_2^{1.5})\}$. The C^1-continuous failure envelope fixes the triaxial strength in stress space in terms of a curvilinear triple-symmetric cone depicted in **Fig.4**, and is expressed as:

$$F(\xi,\rho,\theta)_{fail} = \frac{\rho r(\theta,e)}{\sigma_c} - \frac{\rho_1}{\sigma_c}\left(\frac{\xi-\xi_0}{\xi_1-\xi_0}\right)^{\alpha} = 0 \qquad (19)$$

described by the exponent $\alpha = 0.77$, which determines the shape of the curvilinear meridian to be flatter than a quadratic parabola (i.e., $\alpha = 0.5$). Here, $\xi_0 = \sqrt{3}\sigma_t$ and $\xi_1 = \sqrt{3}S\sigma_c k$, σ_c and σ_t are uniaxial concrete compressive and tensile stresses and parameter S depends on the hardening parameter $0 \le k \le 1$. Also, $\rho_1 = \rho_{uc}/\{(\xi_{uc}-\xi_0)/(\xi_1-\xi_0)\}^{\alpha}$ whereby subscript uc indicates uniaxial compression. The shape of the deviatoric trace is described by the radial distance from the hydrostat[8)]

$$r(\theta,e) = \frac{4(1-e^2)\cos^2\theta + (2e-1)^2}{2(1-e^2)\cos\theta + (2e-1)\sqrt{4(1-e^2)\cos^2\theta + 5e^2 - 4e}} \qquad (20)$$

where the eccentricity $0.5 \le e \le 1.0$ describes the out-roundedness of the deviatoric strength as a hyperbolic function of hydrostatic stress,

$$e = 1 - 0.5(\xi_o - 5.5\sigma_c)/(\xi - 5.5\sigma_c) \qquad (21)$$

To obtain peak stresses, we solve Eqn.(18) for σ_{p3}, while σ_{p1} and σ_{p2} are known and are equal to the current stresses σ_1 and σ_2.

4. PEAK STRAIN CRITERION

To evaluate the concrete lattice peak strain associated with the peak stresses of the lattices $(\sigma_{p1},\sigma_{p2},\sigma_{p3})$, we use fundamental concrete properties. Analysis of the experimental data shows that approximately unique relationships exist between octahedral normal strain and octahedral normal stress, and also octahedral shear strain and octahedral shear stress at the compressive strength[10)]. Based on regression analysis following expressions are given (Ahmad and Shah[10)]):

$$\gamma_{oct} = [-4.86 + 12.76\frac{\tau_{oct}}{\sigma_c}](\gamma_{oct})_0 \qquad (22)$$

$$\varepsilon_{oct} = \left[0.198\left(\frac{\varepsilon_0}{\sigma_0}\right)\right]\sigma_{oct} \qquad (23)$$

Here,

$$(\gamma_{oct})_0 = 0.003(\sigma_0)^{0.13}$$

$$\varepsilon_0 = 0.002 + 0.0007\sigma_0$$

σ_0 = Uniaxial compressive strength of concrete (Mpa). τ_{oct} and σ_{oct} can be calculated from the three lattice stresses of an element as:

$$\tau_{oct} = \frac{1}{3}\left[(\sigma_{p1}-\sigma_{p2})^2 + (\sigma_{p2}-\sigma_{p3})^2 + (\sigma_{p3}-\sigma_{p1})^2\right]$$

$$\sigma_{oct} = \frac{1}{3}(\sigma_{p1}+\sigma_{p2}+\sigma_{p3})$$

Now, we have,

$$\gamma_{oct} = \frac{2}{3}\left[(\varepsilon_{p1}-\varepsilon_{p2})^2 + (\varepsilon_{p2}-\varepsilon_{p3})^2 + (\varepsilon_{p3}-\varepsilon_{p1})^2\right] \qquad (24)$$

$$\varepsilon_{oct} = \frac{1}{3}(\varepsilon_{p1}+\varepsilon_{p2}+\varepsilon_{p3}) \qquad (25)$$

To evaluate all three peak strains, a third equation is necessary which is based on the coaxiality of the deviatoric stress and strain vectors and can be expressed as:

$$\frac{2\sigma_{p2}-\sigma_{p1}-\sigma_{p3}}{2\sigma_{p1}-\sigma_{p2}-\sigma_{p3}} = \frac{2\varepsilon_{p2}-\varepsilon_{p1}-\varepsilon_{p3}}{2\varepsilon_{p1}-\varepsilon_{p2}-\varepsilon_{p3}} \qquad (26)$$

Solving Eq.(24), (25) and (26), we can get the values of $(\varepsilon_{p1},\varepsilon_{p2},\varepsilon_{p3})$. Therefore, we can have completely defined peak point for each of the lattices, with known peak stress and strain. Hence, the complete model in *LECM* to calculate stress from strain in any calculation point can schematically be shown by the following flow chart in **Fig.5**.

5. STRESS STRAIN RELATION FOR CONCRETE LATTICE

With defined peak point for individual lattices, we now establish definitive stress-strain behavior of individual lattices so that tangent value of Young's Modulus as in Eqn.(9) and (18) can conveniently be measured. In this work the following equation proposed by Sargin[7)] is used,

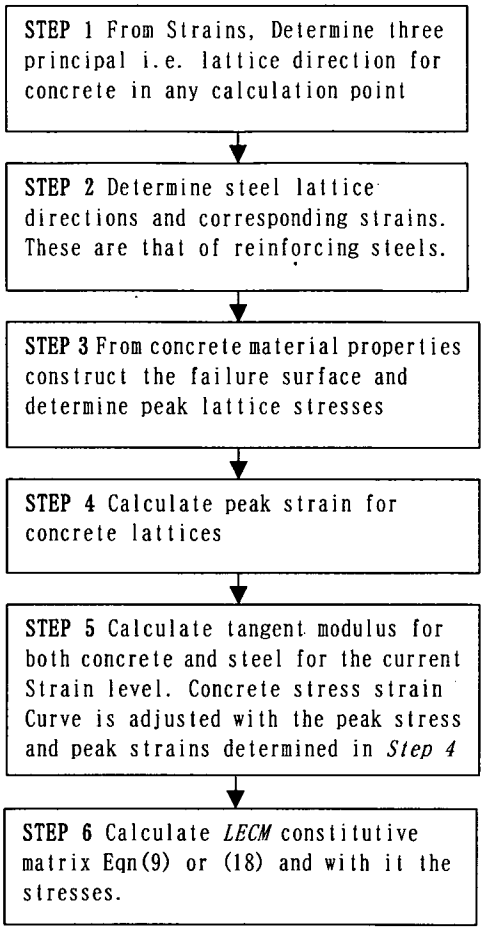

Fig. 5 Flow chart for *LECM* model

$$-\frac{\sigma_c}{\sigma_{pi}} = \frac{-A\frac{\varepsilon}{\varepsilon_{pi}} + (D-1)\left(\frac{\varepsilon}{\varepsilon_{pi}}\right)^2}{1-(A-2)\frac{\varepsilon}{\varepsilon_{pi}} + D\left(\frac{\varepsilon}{\varepsilon_{pi}}\right)^2} \qquad (27)$$

By differentiating, Eq.(27) can be solved to obtain the actual tangent value, which is shown schematically in **Fig.6**, E_t of Young's modulus is given as:

$$E_t = \frac{d\sigma}{d\varepsilon} = \frac{M * N - P * Q}{M^2} \qquad (28)$$

where,

$$P = A\frac{\varepsilon}{\varepsilon_{pi}}\sigma_c - (D-1)\left(\frac{\varepsilon}{\varepsilon_{pi}}\right)^2 \sigma_c$$

$$Q = 2D\frac{\varepsilon}{\varepsilon_{pi}^2} - \frac{A-2}{\varepsilon_{pi}^2}$$

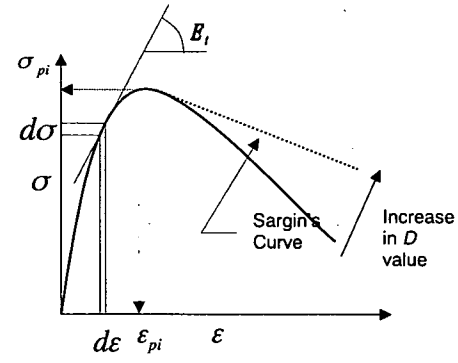

Fig.6 Evaluation of E_t and control of Post-Failure Behavior by Means of Parameter D in Eq.(29)

and,

$$M = 1-(A-2)\frac{\varepsilon}{\varepsilon_{pi}} + D\left(\frac{\varepsilon}{\varepsilon_{pi}}\right)^2$$

$$N = A\frac{\sigma_{pi}}{\varepsilon_{pi}} - 2(D-1)\frac{\sigma_{pi}}{\varepsilon_{pi}^2}\varepsilon$$

Tensile stress and elongation are considered positive, and ε_{pi} determines the strain at failure, i.e., $\varepsilon = -\varepsilon_{pi}$ when $\sigma = -\sigma_{pi}$. The parameter A is defined by $A = E_i / E_s$. The Young's modulus E_i and E_c are initial and the secant modulus at failure, respectively; in which $E_s = \sigma_{pi} / \varepsilon_{pi}$ and D = the parameter which controls the descending part of the stress strain curve. To predict tangent modulus during any load increment from Eq.(29), four parameters are needed: (i) peak strength, σ_{pi} (ii) peak strain ε_{pi} at strength σ_{pi} (iii) the initial slope, E_i, of the stress strain curve and (iv) the parameter, D. σ_{pi} and ε_{pi} are peak lattice stress and strain and can be determined according to the procedure given in section 3 and 4. Initial slope of the stress-strain curve can be determined by the expression like as follows[10]:

$$E_{i3} = E_{i0}\left[1 + 0.31\left(\frac{\sigma_{p1}}{\sigma_0}\right) + \left(\frac{\sigma_{p2}}{\sigma_0}\right)\right] \qquad (29)$$

where, E_{i3}= initial slope for $\sigma_3 - \varepsilon_3$ curve and E_{i0} is the initial slope for uniaxial concrete.

The parameter D determines the post failure behavior of the stress strain curve but the exact form of this curve is unknown and is not obtained by

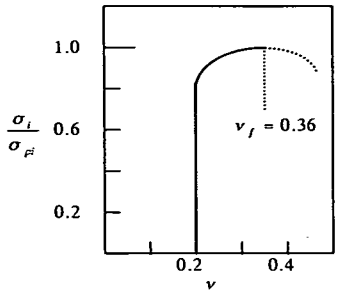

Fig. 7 Variation of Poisson's ratio

standard uniaxial compressive test. Therefore, the actual value of D is chosen in a way so that a convenient post failure curves results. For example the proposed equation by Saenz[11] follows when D=1 in Eq.(26); the Hognestad[12] parabola results when A=2 and D=0 in Eq.(27); and Desayi and Krishnan[13] suggested Eq.(27) with A=2 and D=1.In summary, different post failure behaviors can be simulated by means of parameter D and it only affects the behavior before failure insignificantly. The effect of changing D value is schematically shown in **Fig.6**, where increase in D only changes post failure part of the curve.

6. POISSON'S RATIO

In this work, numerical value of poisson's ratio is been linked with the minimum or maximum (for all tension case) lattice stress of an element in line with proposed method by Ottosen[8]. Since behavior of concrete for uniaxial and triaxial compressive loading is compaction followed by dilation, therefore, poisson's ratio before failure stress is taken as,

$$\nu = \nu_i \qquad when \quad \sigma_i \le 0.8\sigma_{pi}$$

$$\nu = \nu_i - (\nu_f - \nu_i)\sqrt{1-\left(\frac{\sigma_i/\sigma_{pi} - 0.8}{1-0.8}\right)^2} \qquad (30)$$

$$when \quad \sigma_i \ge 0.8\sigma_{pi}$$

Where, σ_i is the maximum/minimum lattice stress and σ_{pi} being the expected failure stress of that lattice as derived in section (3). ν_i and ν_f is poisson's ratio at initial and failure state. ν_f is taken to be as 0.36 in this work. Eq. (30) is shown in **Fig.7**. The second of these equations, which represents one quarter of an ellipse, is only valid up until failure. After failure, although only little is known of the increase in the numerical value of poisson's ratio, it is experimental fact that dilation continues here. Therefore, in the

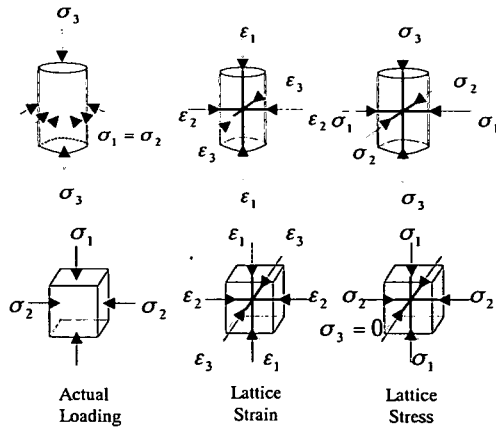

Fig.8 Lattice Idealization of Biaxial and Triaxial Loading

analysis, as E_t is decreased in each step in the post peak region, there is a value of poisson's ratio ν^* such that corresponding bulk modulus, $\kappa = E_t/3(1-\nu^*)$ is unchanged from the previous step. To make provision for dilation to continue in this region ν is taken to be as $1.005\nu^*$ i.e. an increase of 0.5% from no dilation condition, i.e. constant bulk modulus condition. Maximum possible value of poisson's ratio in this work is taken to be as 0.5. i.e. $\nu \le 0.5$ always holds true.

7. COMPARISON WITH EXPERIMENTS

The experimental and predicted stress strain responses using both static and kinematic constraints under biaxial and triaxial loading are shown in **Fig.9**, **Fig.10**, **Fig.11** and **Fig.12** while lattice idealization of biaxial and triaxial cases is shown in **Fig.8**. Only specimens with plain concrete are dealt in this paper. However, for reinforced concrete, procedure is same with three additional lattices contributing in the formation of constitutive matrix (9) and (18). Strains and stiffness of these additional lattices will follow the behavior of reinforcement. The procedure for calculating analytical stress strain curves can be summarized as: (i) For known values of stresses ($\sigma_1 and \sigma_2$) calculate the peak strength of lattices ($\sigma_{p1}, \sigma_{p2}, \sigma_{p3}$) as described in section (3). (ii) Knowing the values of peak strength, calculate peak strains ($\varepsilon_{p1}, \varepsilon_{p2}, \varepsilon_{p3}$) using Eqns. (24),(25) and (26). (iii) Calculate the initial slope E_i using Eqn.(29) and thus $A(=E_i/E_c)$ (iv) Calculate the tangent modulus of concrete by appropriately selecting the parameter D. (v) Calculate the complete stress strain curve using

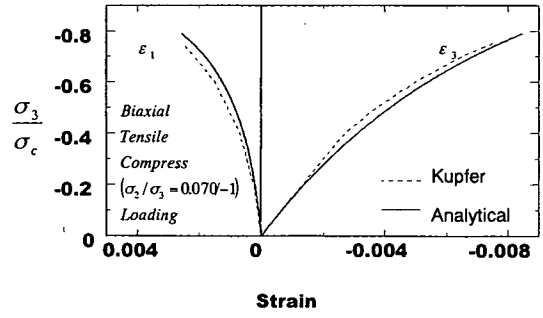

(a) Biaxial tensile-Compressive Loading

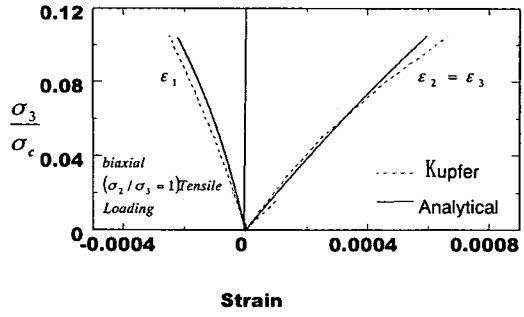

(a) Tensile loadings

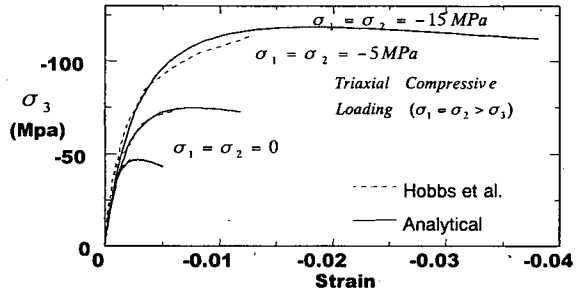

(b) Triaxial Compressive Stress State :Hobbs et al.[16]

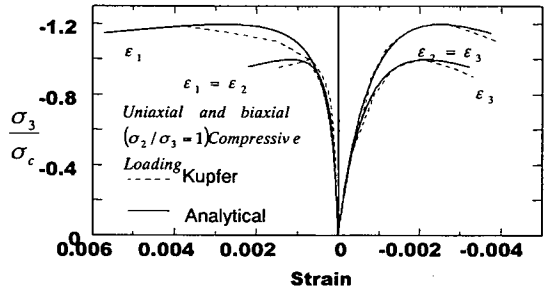

(b) Biaxial Compressive Loading

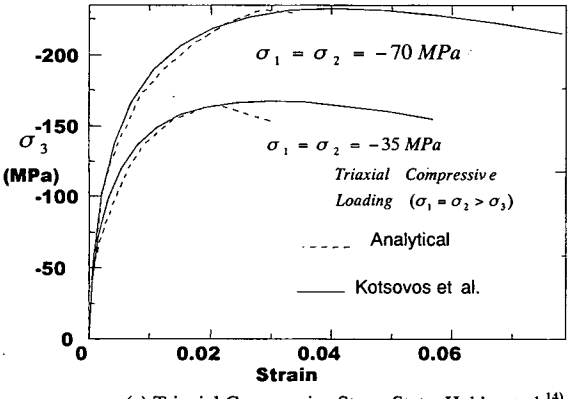

(c) Triaxial Compressive Stress State: Hobbs et al.[14]

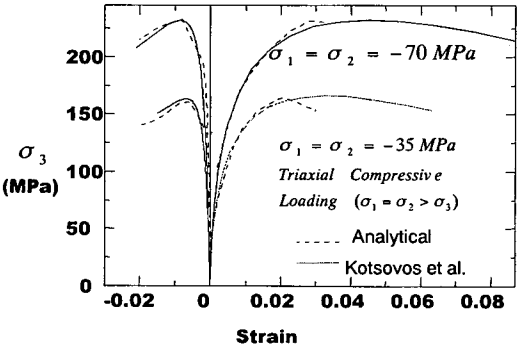

(c) Triaxial Compressive Stress State: Hobbs et al.[14]

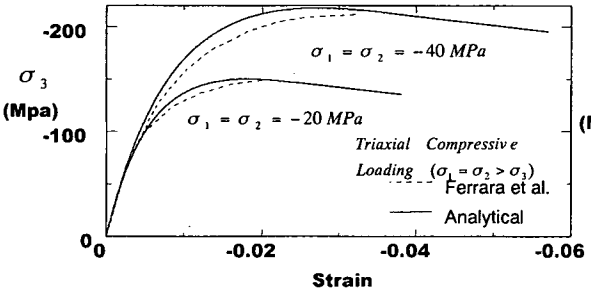

(d) Triaxial Compressive Stress State: Ferrara et al.[13]

Fig.9 Comparison with Experimental Results: Kinematic Constraint

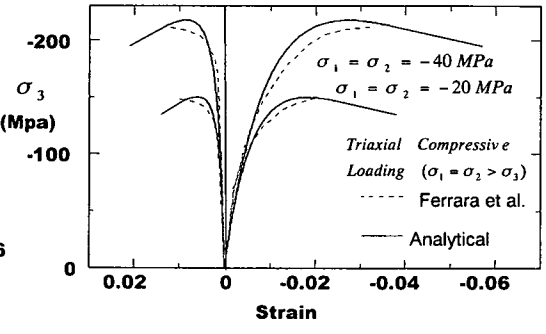

(d) Triaxial Compressive Stress State: Ferrara et al.[13]

Fig.10 Comparison with Experimental Results: Static Constraint

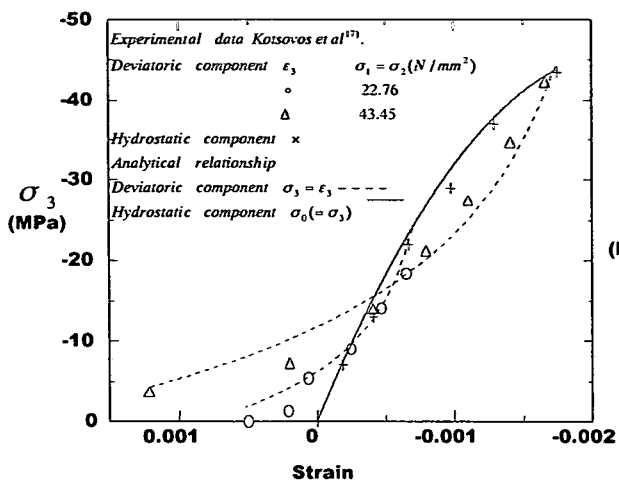

Fig.11 Stress-strain relationship for concrete under various state of stress: Kinematic Constraint

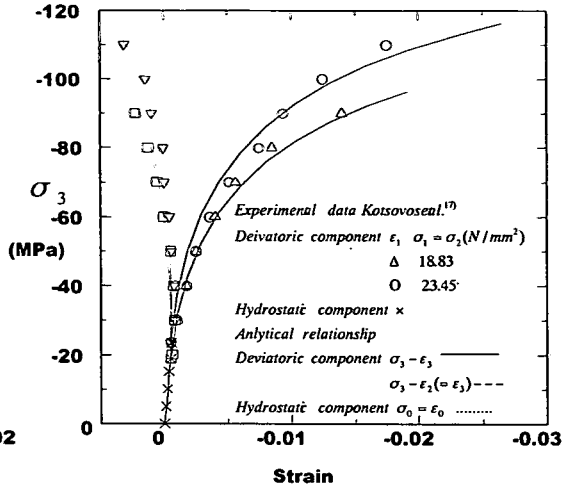

Fig.12 Stress-strain relationship for concrete under various state of stress: Static Constraint

Table 1 Concrete parameters

	σ_c (Mpa)	σ_t (Mpa)	ε_c	ν_i	D
Ferrera et al.[13]	56.9	4.55	0.0021	0.16	0.26
Hobbs[14]	43.4	3.47	0.0022	0.20	0.10
Kotsovos et al.[16]	62.0	4.96	0.0025	0.18	0.20
Kupfer[15]	18.7	1.87	0.0018	0.19	0.00

Table 2 Comparisons of Peak Points

	Peak Stress (MPa)		Peak Strain	
	Exp.	Anl.	Exp.	Anl.
Ferrara et al.[13] $\sigma_1 = \sigma_2 = -40MPa$	-209	-221	-.032	-.027
Kotsovos et al.[16] $\sigma_1 = \sigma_2 = -70MPa$	-257	-268	-.028	-.037
Hobbs et al.[14] $\sigma_1 = \sigma_2 = -5MPa$	-73	-76	-.0057	-.007

the governing constitutive Eqn. (9) or (18) .

Experimental observations by Ferrara et al.[14], Hobbs[15], Kupfer[16] and Kotsovos et al.[17] are used in this work as measure of comparison of the derived constitutive laws. Experimental works are chosen in a way so that it covers wide range of stress states including tensile and high hydraulic stresses with concrete strength varying from low to of very high strength. Concrete parameters used in analyzing these experiments are shown in **Table 1**. These parameters are taken from the test report of respective experiments. Apart from σ_c and σ_t, other three parameters required to construct the failure surface are taken as: $e = e(\xi)$, $\alpha = 0.77$ and S=7.0 according to Kang and Willam[5)6)]. Note that value of D ranges from 0~0.26 and is merely chosen manually so as to make post peak portion of the stress strain curve as close as close possible to the experimental observations. For general cases, where post peak strain softening is an expected outcome, value of D in the range of 0.15~0.30 is appropriate. For expected brittle failure in shear or tension, D value should be taken close to zero.

The biaxial stress results of Kupfer[16] are considered first. **Fig.9(a), 10(a)** and **10(b)** show comparison between the predictions of the proposed laws to experimental results. Concrete is of low strength. **Fig.9(a)** is of tensile compressive loading; response evaluated by kinematic constraint equation (9). **Fig.10(a)** and **10(b)** are that of biaxial tension and compression respectively; analytical responses are derived from static constraint equation (18). The behavior of concrete becomes less nonlinear, the more the stress state involves tensile stresses, as can be seen from these figures. The loading in figures **9(a)** and **10 (a)** results in complete brittle failure. Stress strain curves for triaxial compressive loading resulting in failure along compressive meridian are shown in **Fig.9(b), (c), (d)** and **10(c), (d)**. The experimental results of **Fig. 9(b), (c)** and **(d)** are those of Hobbs et al.[15], Kotsovos et al.[17] and Ferrara et al.[14] respectively. Concrete is of moderate strength for the case of Hobbs[15] but of very high strength for both the cases of Kotsovos[17] and Ferrara[14]. The analytical results for these experiments are form Kinematic constraints method (Eq.9). **Figs. 10(c)** and **(d)** represent experimental and analytical results of Kotsovos[17] and Ferrara[14] respectively. Even though no experimental data exists, analytical stress strain curves on these figures are also shown at the

beginning of the post failure region to indicate their shape. Special attention should be given to **Fig9(c)**, **10(c)** and **Fig.9(d)**, **10(d)** where same experimental curve is reproduced using both kinematic (Eq.9) and static constraint (Eq.18) methods. As can be seen from these two sets of graphs, analytical responses for both static and kinematic constraint method are almost exactly same for same parameters used with same number of computational steps. However, it should be noted that lateral strain couldn't be evaluated for the case of kinematic constraint method (Eq.9). This is because for these simple cases, where only three mutually perpendicular concrete lattices are involved, the non-diagonal elements of the rigidity matrix of kinematic constraint are zero. This makes lattices to be insensitive to the strains to lattices in other directions. This, however, does not occur for static constraint method (Eq.18), where poisson's ratio contributes to non-diagonal elements. Therefore, we can conclude, although kinematic constraint rigidity matrix give accurate enough results for the loading direction in question as can be seen here and as was shown for 2D cases[2], static constraint rigidity matrix is more comprehensive and complete in its characteristics due to inclusion of poisson's ratio.

Typical comparison between experimental peak and strain with analytical peak stress and strain are given in **Table 2** for quick comparison. While analytical peak stresses remained within 10% of the experimental results, peak strain varied in between 10% to 20%. As can be seen from the **Fig.9** and **10**, the analytical curves predict the experimental results favorably, which establishes effectiveness of the proposed constitutive laws. Furthermore, some discrepancies may due to minor difference between predicted peak stress and strain and actual ones than to the governing constitutive equation itself.

Next we check whether the developed constitutive laws can actually simulate the stress-strain relation of entire loading sequence. Prescribed loading path essentially consists of two parts[17] (i) Increasing the hydrostatic stress up to a given value; and then (ii) application of axial compressive stress to failure $(\sigma_3 < \sigma_2 = \sigma_1)$ or, applying tensile stresses to failure $(\sigma_3 > \sigma_1 = \sigma_2)$. As shown in **Fig.11**, hydrostatic loads are given up to 43.45 MPa; and axial tensile load is given on two points, one at 22.76 Mpa and the other at 43.45 MPa. Analysis results are that of kinematic constraint constitutive laws. While in **Fig.12** hydrostatic loads are given up to 23.45 MPa and axial compressive loads are increased at two point: 18.83MPa and 23.45 MPa [17]. Analytical results are based on static constraint method. In both of the cases, as we can see from the figures developed constitutive laws are quite effective in simulating entire stress strain path, confirming once again the validity of the derived constitutive laws.

8. CONCLUDING REMARKS

Three-dimensional constitutive laws based on *LECM* are formulated and presented in this paper. Two fundamentally different constitutive laws are derived using the concept: one from kinematic constraints and the other from static constraints. Analytical results are calculated using these laws for experiments that cover wide range of stress states and obtained using different types of concrete in terms of their strength. Through these examples of biaxial and triaxial test analysis data, it is shown here that uniaxial lattice representation of concrete and its' corresponding equivalent continuum i.e. *LECM* can effectively capture the behavior of stress-strain response in three-dimensions. Furthermore, simple and transparent formulation of the constitutive matrix enables us to recognize the sensitivity of each of the lattices in an element and thereby gives insight into the response characteristics and complex behavior of concrete in a simplistic way.

REFERENCES

1) Selby, R. G. and Vecchio, F. J.: Three-dimensional Constitutive Relations for Reinforced Concrete, *Publ. No. 93-02, Dept of Civil Engrg.*, Univ. of Toronto, Canada, 1993.
2) Tanabe, Tada-aki and Ahmad, Syed Ishtiaq: Development of Lattice Equivalent Continuum Model for Analysis of Cyclic Behavior of Reinforced Concrete, *ASCE special publication on Modeling of Inelastic Behavior of RC structures under Seismic Loads*, pp.297-314, 2000
3) Niwa, J., Choi, I.C., and Tanabe, T.: Analytical Study for Shear Resisting Mechanism using Lattice Model, *JCI Int. Workshop on Shear in Concrete Structures*, pp. 130-145, June, 1994.
4) Bazant, Z.P. and Prat, P.C.: Microplane Model for Brittle-Plastic Material-parts I and II, Journal of Engineering Mechanics, ASCE, Vol. 114, pp.1672-1702, 1988.
5) Kang, H.D: Triaxial Constitutive Model for Plain and Reinforced Concrete Behavior, *PhD Dissertation, University of Colorado Bourlder*, 1997.
6) Kang, H.D. and Willam, K.: Mechanical Properties of Concrete in Uniaxial Compression, *Materials Journal, American Concrete Institute*, Vol. 94, No.6, pp. 457-471, 1997,
7) Sargin, M.: Stress-Strain Relationships for Concrete and the Analysis of Structural Concrete Sections, *Study No. 4, Solid Mechanics Division, University of Waterloo*, Waterloo, Ontario, Canada, 1971.
8) Ottosen, Niels Saabye: Constitutive Model for Short Time Loading of Concrete, *Journal of Engineering Mechanics Division*, ASCE, Vol. 105, pp. 127-141, March, 1978.
9) Willam, K.J. and E.P. Warnke: Constitutive Models for the the Triaxial Behavior of Concrete, *Int. Assoc. Bridge Struct. Eng. Sem. Concr. Struct. Subjected to Triaxial Stresses*, Bergamo, Italy, 1974, Int. Assoc. Bridge Struct. Eng. Proc. Vol. 19, pp. 1-30, 1975.

10) Ahmad, Shuaib H. and Shah, Surendra P.: Complete Triaxial Stress-Strain Curves for Concrete, *Journal of Structural Engineering Division*, ASCE, Vol. 108, pp. 728-742, March, 1982.
11) Saenz, L. P.: discussion of "Equation for the Stress-Strain Curve of Concrete" by Desayi and Krishnan, *Journal of the American Concrete Institute*, Vol. 61, pp. 1229-1235, Sept., 1964.
12) Hognestad, E.: A Study of Combined Bending and Axial Load in Reinforced Concrete Members, *Engineering Experment Station, University of Illinois*, Bulletin Series No. 399, Urbana, Ill., Nov., 1951.
13) Desayi, P. and Krishnana, S.: Equation for the Stress-Strain Curve of Concrete, *Journal of the American Concrete Institute*, Vol. 61, No.3, pp. 1169-1183, Mar., 1964.
14) Ferrari, G., Rossi, P., Rossi, P.P., Ruggeri, L.: Dispositivi di prova per l'analisi sperimentale del comportamento di conglomerati cementizi sottoposti a stati triassiali di dollecitazione, *Proceedings of 4th Associazione Italiana Annalisi Sollecitazione Congress*, Rome, Italy, Oct., 1976.
15) Hobbs, D.W.: Strength and Deformation Properties of Plain Concrete Subject to Combined Stress, *Cement and Concrete Association*, Part 3, Technical Report 42.497, London, England, 1974.
16) Kupfer, I.D., and Jirsa, J.O.: Behavior of Concrete under Compressive Loadings, *Journal of the American Concrete Institute*, Vol.66, No. 8, pp.656-666, Aug., 1969.
17) Kotsovos, M.D. and Newmann, J. B.: Generalized Stress-Strain Relation for Concrete, *Journal of Engineering Mechanics Division*, ASCE, Vol.99, pp. 853-866, Aug., 1973.

(Received 2001.10.1)

3次元格子等価連続体に基づくコンクリート構成則の構築

サイド　イスティアック　アハマド・　田辺　忠顕

格子システムを等価な連続体に導くことにより，簡便で，数値解析上の安定性が高く，設計者に望まれる3次元コンクリート構成則の定式化を行った．本研究では，構成則の定式化に際し，2つの手法を用いている．一つは，ひずみ場から定式化される構成則であり，もう一つは応力場から得られる構成則である．特に後者では，ポアソン比を評価することが可能となる．また，各コンクリート格子成分の等価一軸応力－ひずみ挙動の提案も行った．構築された構成則を，様々な研究者らの2軸，3軸試験の数値解析に適用した結果，解析結果は実験結果と良い一致を示し，提案する構成則の有効性が確認された．